nanomaterials

MDPI

Article

Synthesis and Enhanced Ethanol Gas Sensing Properties of the g-C_3N_4 Nanosheets-Decorated Tin Oxide Flower-Like Nanorods Composite

Yan Wang [1,2], Jianliang Cao [3,*], Cong Qin [3,*], Bo Zhang [3], Guang Sun [3] and Zhanying Zhang [3]

1 The Collaboration Innovation Center of Coal Safety Production of Henan Province, Jiaozuo 454000, China; yanwang@hpu.edu.cn
2 State Key Laboratory Cultivation Bases Gas Geology and Gas Control (Henan Polytechnic University), Jiaozuo 454000, China
3 School of Chemistry and Chemical Engineering, Henan Polytechnic University, Jiaozuo 454000, China; zhb@hpu.edu.cn (B.Z.); mcsunguang@hpu.edu.cn (G.S.); zhangzy@hpu.edu.cn (Z.Z.)
* Correspondence: caojianliang@hpu.edu.cn (J.C.); qincongxy@163.com (C.Q.); Tel.: +86-391-398-7440 (J.C. & C.Q.)

Received: 23 August 2017; Accepted: 18 September 2017; Published: 22 September 2017

Abstract: Flower-like SnO_2/g-C_3N_4 nanocomposites were synthesized via a facile hydrothermal method by using $SnCl_4 \cdot 5H_2O$ and urea as the precursor. The structure and morphology of the as-synthesized samples were characterized by using the X-ray powder diffraction (XRD), electron microscopy (FESEM and TEM), and Fourier transform infrared spectrometer (FT-IR) techniques. SnO_2 displays the unique 3D flower-like microstructure assembled with many uniform nanorods with the lengths and diameters of about 400–600 nm and 50–100 nm, respectively. For the SnO_2/g-C_3N_4 composites, SnO_2 flower-like nanorods were coupled by a lamellar structure 2D g-C_3N_4. Gas sensing performance test results indicated that the response of the sensor based on 7 wt. % 2D g-C_3N_4-decorated SnO_2 composite to 500 ppm ethanol vapor was 150 at 340 °C, which was 3.5 times higher than that of the pure flower-like SnO_2 nanorods-based sensor. The gas sensing mechanism of the g-C_3N_4nanosheets-decorated SnO_2 flower-like nanorods was discussed in relation to the heterojunction structure between g-C_3N_4 and SnO_2.

Keywords: nanocomposites; microstructure; gas sensor; flower-like SnO_2 nanorod; graphitic carbon nitride

1. Introduction

As an n-type metal-oxide semiconductor, tin oxide (SnO_2) has wide applications in many fields, such as lithium-ion batteries [1], photocatalysis [2], and gas sensors [3]. SnO_2 has been investigated as a typical semiconductor gas sensor to ethanol because of its unique chemical properties and crystal structure [4]. As is known, the gas-sensing performance of SnO_2-based sensors can be improved by means of morphology and size control. Hence, diverse shape-controlled SnO_2 nanostructures have been synthesized, such as nanoflower [5], nanoarray [6], nanoplate [7], and nanowire [8]. These SnO_2-based sensors exhibited good sensing properties, including low-cost and fast response and recovery.

However, there are some limitations which prevent the direct application of these sensors, such as poor electrical characteristics, high work temperature, and a low response [9]. Coupling SnO_2 with other semiconductors to construct the heterojunction structure could be an efficient way to overcome these disadvantages. Therefore, many SnO_2-based composites such as SnO_2/r-GO [10–15], SnO_2/ZnO [16–19], SnO_2/Fe_2O_3 [20–23], and SnO_2/NiO [24–26] have been synthesized as

high-efficiency gas sensors. Graphitic carbon nitride (g-C_3N_4) is a two-dimensional (2D) semiconductor with a 2.7 eV band gap, which possesses good chemical stability and a large surface area. It is available to form an n/n junction structure with SnO_2 [27]. For example, SnO_2/g-C_3N_4nanocomposites with a strong heterojunction structure were designed and fabricated. The photocatalytic activity of the SnO_2/g-C_3N_4 nanocomposites exhibited enhanced catalytic activity and stable cycle property [28]. Zhang et al. prepared the α-Fe_2O_3/g-C_3N_4 heterostructural nanocomposites as an ethanol gas sensor, and the composites exhibited a high response value (S = 7.76) to 100 ppm ethanol under a working temperature of 340 °C [29]. Zeng et al. successfully fabricated the α-Fe_2O_3/g-C_3N_4 composites for the cataluminescence sensing of H_2S [30]. An efficient dielectric barrier discharge (DBD) plasma-assisted method for the fabrication of the g-C_3N_4-Mn_3O_4 composite was investigated by Hu et al., which displayed a highly selective, sensitive, and linear cataluminescence (CTL) response towards H_2S gas [31]. Sanjay Mathur et al. synthesized SnO_2 nanowires via the CVD method, and the SnO_2 nanowires exhibited an excellent photoresponse performance [32]. Kuang et al. have synthesized high-yield SnO_2 nanowires via an Au catalytic vapor-liquid-solid (VLS) growth process and the SnO_2 nanowire-based humidity sensor displayed a fast response and high sensitivity to relative humidity changes at room temperature [33]. The three-dimensional network's SnO_2 nanowire was prepared via a flame-based thermal oxidation process (FTS) and applied for ethanol sensing [34]. Oleg Lupan et al. investigated the hybrid networks of heterogeneous shell-core Ga_2O_3/GaN:O_x@SnO_2 nano- and micro-cables with a shell in mixed phases for improving sensor properties [35]. However, to our best knowledge, there is still no research focused on the design and gas sensing application of the g-C_3N_4 nanosheets-decorated SnO_2 flower-like nanorods.

Herein, the hydrothermal method was utilized for the first time to synthesis the g-C_3N_4 nanosheets-decorated SnO_2 flower-like nanorods for the ethanol sensing application. It was found that the g-C_3N_4 nanosheets-decorated tin oxide flower-like nanorods composite possesses a much higher response value, repeatability, and stability to ethanol vapor than pure flower-like SnO_2 nanorods.

2. Results and Discussion

2.1. Sample Characterization

The pure SnO_2 and SnO_2/g-C_3N_4 composites with 5, 7, and 9 wt % g-C_3N_4 contents were synthesized by a facile hydrothermal method. Also, the as-prepared samples were marked as SnO_2/g-C_3N_4-5, SnO_2/g-C_3N_4-7, and SnO_2/g-C_3N_4-9, respectively. Figure 1 displays the XRD patterns of the synthesized SnO_2, g-C_3N_4, and g-C_3N_4nanosheets-decorated tin oxide flower-like nanorods (SnO_2/g-C_3N_4) composites with different g-C_3N_4 contents. One can see from the XRD pattern that two diffraction peaks at 13.1° and 27.5° can be observed for pure g-C_3N_4;these two peaks were accorded to the (100) plane and (002) plane of g-C_3N_4,which could be due to the inter-layer structure of the tri-s-triazine unit with interplannar spacing and the conjugated aromatic system, respectively [36]. The XRD patterns of SnO_2/g-C_3N_4 composites show some diffraction peaks at 26.61°, 33.89°, 37.94°, and 51.78°, which could be assigned to the (110), (101), (200), and (211) planes of the tetragonal rutile structure SnO_2 (JCPDS Card No. 41-1445). However, the diffraction peaks of g-C_3N_4 are not observed in the SnO_2/g-C_3N_4 composites. This could be due to the small content of g-C_3N_4.

The microstructure and morphology of the synthesized samples were verified by using FESEM and TEM. One can see clearly from Figure 2a that the morphology of the as-prepared g-C_3N_4 possesses many wrinkles with overlaps at the edges, demonstrating the existence of the two dimensional (2D) nano-lamellar structure. It can be observed from Figure 2b that the pure SnO_2 product displays the unique 3D flower-like microstructure assembled with many uniform nanorods. The lengths and diameters of a single nanorod are about 400–600 nm and 50–100 nm, respectively. For the g-C_3N_4 nanosheets-decorated SnO_2 flower-like nanorods composite, as shown in Figure 2c, the SnO_2 flower-like nanorods were closely coupled by g-C_3N_4 nanosheets. A proposed growth mechanism of SnO_2 flower-like nanorods can be summarized by crystal growth and nucleation

theory. The SnO_2nanocrystals nucleation points are generated in different orientations. Therefore, the SnO_2 nanorods grow in irregular directions and finally formed into 3D flower-like structures. Figure 2f displays the typical TEM image of pure g-C_3N_4, and g-C_3N_4possesses two dimensional nanosheets structure with many wrinkles. The TEM images of g-C_3N_4 nanosheets-decorated tin oxide flower-like nanorods composites are displayed in Figure 2d,e, and SnO_2 flower-like nanorods were coupled by a lamellar structure, which is 2D g-C_3N_4. Thus, we can conclude that g-C_3N_4 nanosheets-decorated SnO_2 flower-like nanorods composites were successfully synthesized by the hydrothermal method combining the above analysis results offered by XRD, FESEM, and TEM.

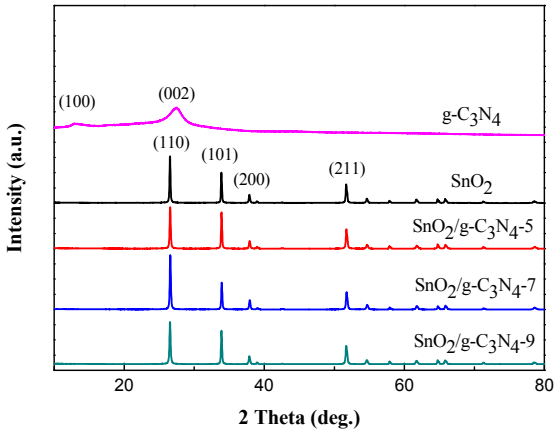

Figure 1. X-ray powder diffraction (XRD) patterns of the synthesized SnO_2, g-C_3N_4, and g-C_3N_4nanosheets-decorated tin oxide flower-like nanorods composites (SnO_2/g-C_3N_4-5, SnO_2/g-C_3N_4-7, and SnO_2/g-C_3N_4-9).

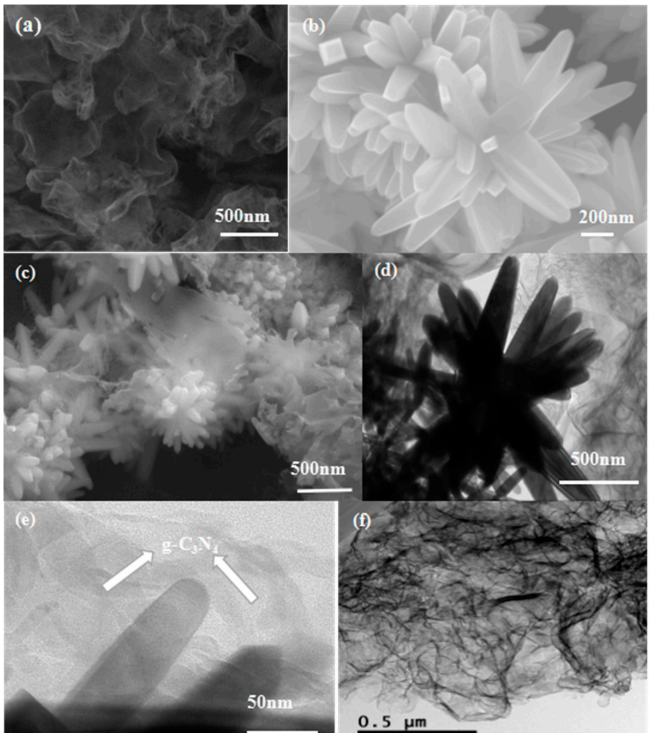

Figure 2. Field-emission scanning electron microscopy (FESEM) images of pure g-C_3N_4 (**a**); SnO_2 flower-like nanorods (**b**); SnO_2/g-C_3N_4nanocomposite (**c**); and transmission electron microscopy (TEM) images of the SnO_2/g-C_3N_4 composite (**d**,**e**) and pure g-C_3N_4 (**f**).

Figure 3 exhibits the FT-IR spectra of g-C_3N_4, SnO_2, and SnO_2/g-C_3N_4-7 samples. As can be seen from Figure 3b, the broad absorption peaks could be observed at wave-numbers of 570 cm^{-1} and 660 cm^{-1}, which could be assigned to the Sn–O characteristic peaks. In Figure 3a,c, the peaks in the range of 1240–1637 cm^{-1} are ascribed to the C–N and C=N stretching vibration modes, and the peak at 808 cm^{-1} corresponds to the triazine units. These two sets of characteristic vibration peaks are characteristic of g-C_3N_4. As is shown in Figure 3c, all the characteristic peaks of SnO_2 and g-C_3N_4 can be observed clearly. These results make up for our XRD analysis, in which g-C_3N_4 and SnO_2 are coexisting in the SnO_2/g-C_3N_4 composites. Compared with pure g-C_3N_4, there is a slight red shift in the bands of g-C_3N_4 in the composite. This result indicates that there is an interaction between SnO_2 and g-C_3N_4 [27], which is beneficial to the gas sensing application.

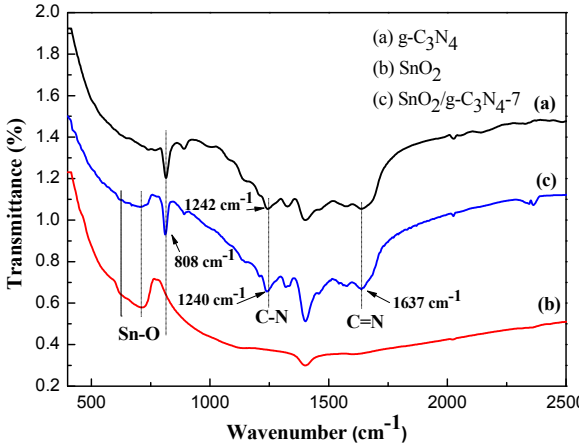

Figure 3. Fourier transform infrared spectrometer (FT-IR) spectra of g-C_3N_4 (**a**); SnO_2 (**b**); and SnO_2/g-C_3N_4-7 (**c**) nanocomposite.

TG analysis was investigated by heating up from room temperature to 800 °C at a heating rate of 5 °C·min^{-1} to reveal the weight change of g-C_3N_4. It can be seen from Figure 4 that the weight of g-C_3N_4 is set constant at temperature below 500 °C. When the temperature increases to 510 °C, the weight of g-C_3N_4 starts to decrease (the combustion of g-C_3N_4 in air). The weight stays at the same level when the temperature exceeds 655 °C. It can be concluded that g-C_3N_4 is stable at low temperature and burn at high temperature. This phenomenon demonstrates that g-C_3N_4 could stably exist in the composite under the operating temperature in the range of 200–400 °C in the gas-sensing test process.

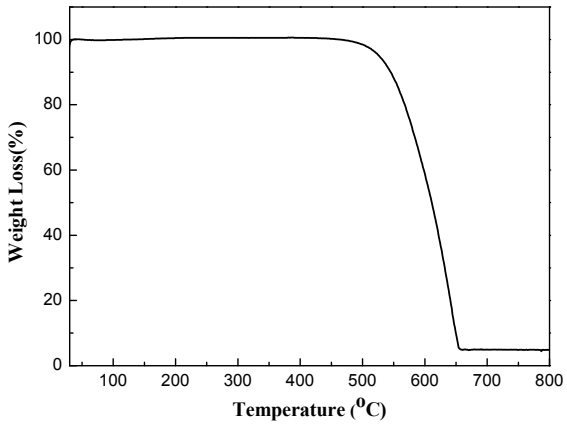

Figure 4. Thermogravimetry (TG) analysis for heating the g-$C_3N_4$from room temperature to 800 °C.

2.2. Sensing Performance Tests

In order to investigate the gas sensing performance of the synthesized samples-based sensor to ethanol, a series of tests were performed. The response values (R_a/R_g) of the g-C_3N_4nanosheets-decorated tin oxide flower-like nanorods composite and the pure flower-like SnO_2-based gas sensors toward 500 ppm ethanol vapor were measured under different operating temperature. With the increase of operating temperature, one can see from Figure 5a that all of the samples exhibited the similar variation tendency. Also, the response values of the SnO_2/g-C_3N_4-based sensors reached the maximum value at 340 °C, while the maximum value of pure SnO_2 was 70 at 360 °C. This result shows that the optimum operating temperature of SnO_2/g-C_3N_4 decreased compared with that of pure SnO_2. This result may be due to the fact that the chemisorbed oxygen species can achieve the required energy and effectively react with ethanol vapor molecules on sample surface varying the resistance significantly [37]. The response value of the SnO_2/g-C_3N_4 composite-based sensor is much higher than pure SnO_2. The response values increased with adding the content of g-C_3N_4 from 5 wt. % to 7 wt. % and decreased with further increase of g-C_3N_4 content. The response values of the pure SnO_2, SnO_2/g-C_3N_4 composites with g-C_3N_4 contents of 5, 7, and 9 wt. % to 500 ppm ethanol vapor at 340 °C are 43, 125, 150, and 135, respectively, indicating that the addition of g-C_3N_4 has a great influence on enhancing the gas sensing performance. When the mass percentage of g-C_3N_4 in the composites is 7 wt. %, the response reaches the maximum value. A suitable content of g-C_3N_4 in the composite is beneficial to form the preferable heterojunction structure in the interface region between flower-like nanorods SnO_2 and 2D g-C_3N_4. However, much higher addition of g-C_3N_4may result in the formation of the connection of bulk. This will further decrease the specific surface area of the sample and reduce the active sites for oxygen and ethanol gas adsorption, further leading to the degradation of sensing performance. Hence, the optimum operating temperature is 340 °C and the optimum g-C_3N_4 content is 7 wt. % for this g-C_3N_4 nanosheets-decorated SnO_2 flower-like nanorods nanomaterial. Therefore, all of the further research was carried out by using SnO_2/g-C_3N_4-7 composite sensor at 340 °C. Figure 5b displays the response values of the four samples to different ethanol vapors in the concentration range of 100–3000 ppm at 340°C. With the increase of ethanol concentration, the response values increased for all of these four sensors. The curves increased rapidly in the range of 100–500 ppm and increased slowly with the increasing concentrations from 500 ppm to 3000 ppm.

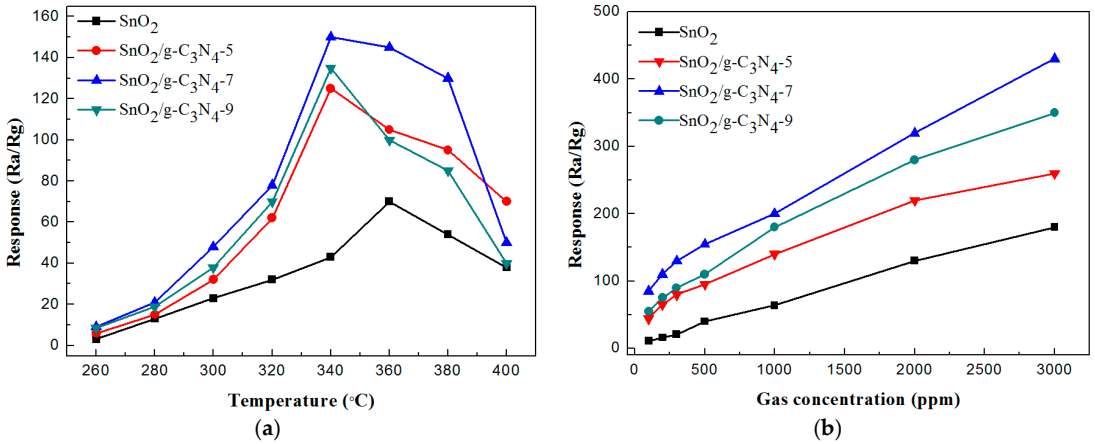

Figure 5. The response values of the SnO_2, SnO_2/g-C_3N_4-5, SnO_2/g-C_3N_4-7, and SnO_2/g-C_3N_4-9 to 500 ppm ethanol (**a**) under different operating temperatures; (**b**) for different concentrations of ethanol at 340 °C.

Figure 6a shows the real time response curves of the pure SnO_2 and SnO_2/g-C_3N_4-7 to ethanol in the range of 100–3000 ppm at 340 °C. All of the response-recovery cycles were measured about 300 s with a response interval and a recovery interval of 150 s, respectively. We can observe from

Figure 6a that the two samples show a similar trend: the response values increase with increasing ethanol concentration. To the same concentration of ethanol, SnO_2/g-C_3N_4-7 exhibited much higher response value than that of pure SnO_2. The response value of the SnO_2/g-C_3N_4-7 composite-based sensor towards 500 ppm ethanol vapor was about 150, about four times higher than pure SnO_2. As is known, response-recovery time is another very important influential factor on the application of gas sensor. Figure 6b shows the response-recovery time curve of the SnO_2/g-C_3N_4-7 composite toward 500 ppm ethanol vapor. As seen from the curve, when the sensor was exposed and separated to ethanol, the response increased rapidly (31 s) and also decreased rapidly (24 s), respectively.

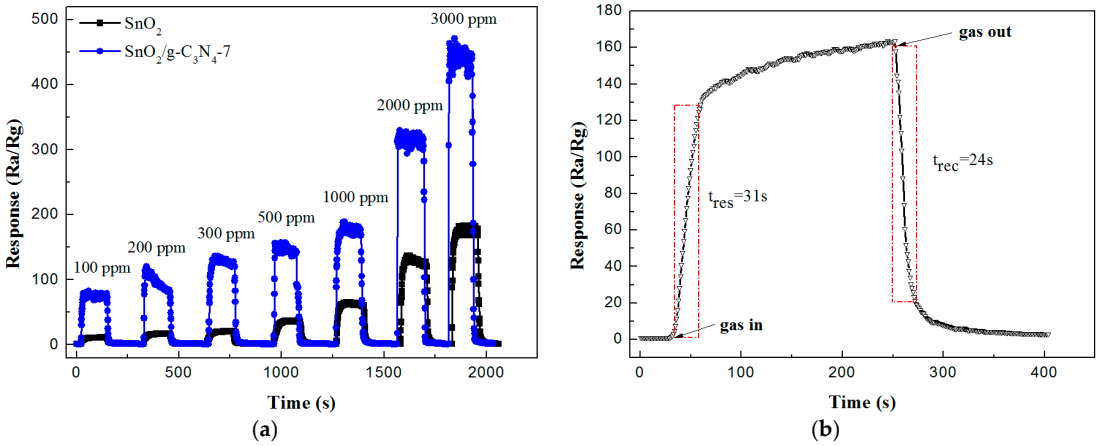

Figure 6. (**a**) The real time response curves of the SnO_2 and SnO_2/g-C_3N_4-7 composite sensors toward ethanol vapor; (**b**) response-recovery time characteristics of the SnO_2/g-C_3N_4-7 based sensor to 500 ppm ethanol vapor at 340 °C.

The repeatability and stability are both crucial influence factors of gas sensing performances. As is shown in Figure 7a, the response values of these four response-recovery cycles of SnO_2/g-C_3N_4-7 sensor stay almost the same (165, 160, 167, and 155) toward 500 ppm ethanol at 340 °C. This result indicated that the synthesized SnO_2/g-C_3N_4-7 composite possesses an admirable repeatability for ethanol vapor detection. Figure 7b displays the stability test result of SnO_2/g-C_3N_4-7 composite sensor toward 500 ppm ethanol vapor at 340 °C, and the response values were kept at a stability of around 155 after 30 days test, indicating that the synthesized g-C_3N_4 nanosheets-decorated SnO_2 flower-like nanorods composite possesses an excellent stability.

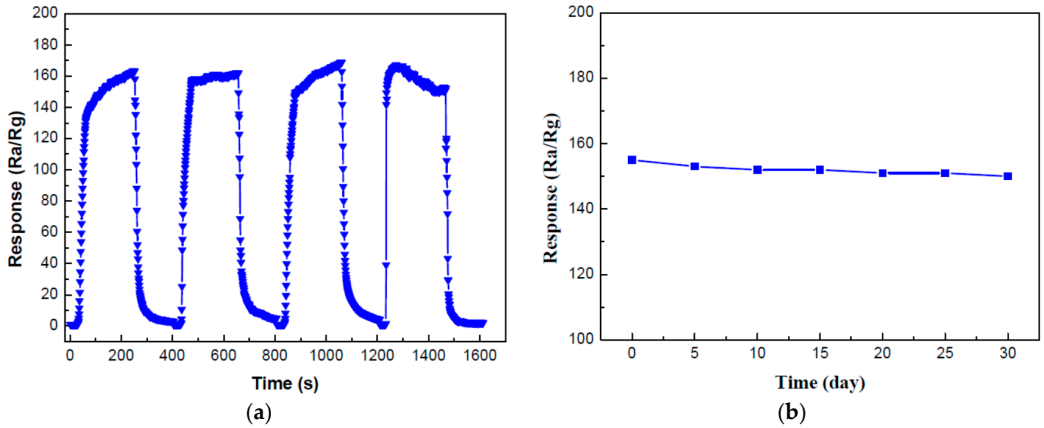

Figure 7. (**a**) Repeatability and (**b**) stability measurements of the SnO_2/g-C_3N_4-7-based sensor to 500 ppm ethanol at 340 °C.

As is well known, the selectivity of the sensor for the different gases is one of the most important factors for its practical application. Figure 8 displays the selectivity test results of SnO_2 flower-like nanorods and SnO_2/g-C_3N_4-7 composite to methanol, ethanol, toluene, formaldehyde, and acetone with the concentration of 500 ppm. The test results indicated that the sample possesses the superior selectivity to ethanol vapor at the operating temperature of 340 °C. The high selectivity to ethanol maybe come from the fact that when reacted with the absorbed oxygen, ethanol is more likely to lose electrons, and hydroxyl group (–OH) is easy to oxidize under the optimum operating condition.

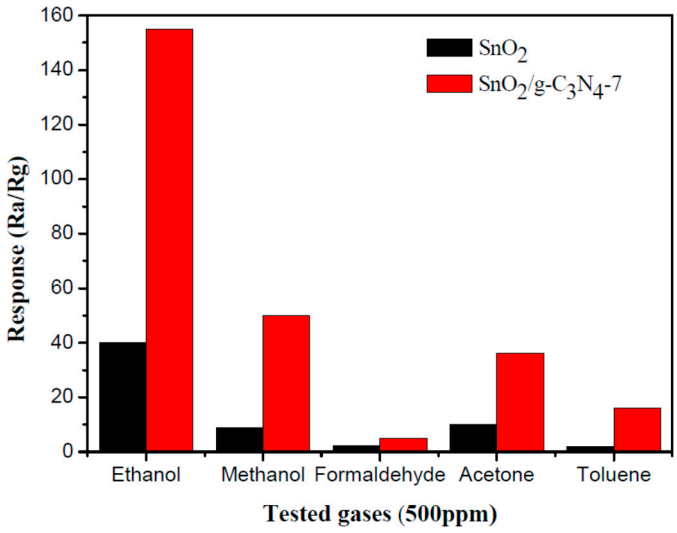

Figure 8. Comparision of the response values of the flower-like SnO_2 nanorods and the SnO_2/g-C_3N_4-7 composite toward 500 ppm different gases at 340 °C.

Table 1 lists the sensing performances of different materials to ethanol vapor. One can observe from Table 1 that the RGO/hollow SnO_2 nanoparticles [11], hollow ZnO/SnO_2 spheres [16], tubular α-Fe_2O_3/g-C_3N_4 [29], and Au/3D SnO_2 microstructure [38] samples possess the response values to ethanol of 70.4, 78.2, 7.76, and 30, respectively. In our research, the 7 wt. % 2D g-C_3N_4 decorated SnO_2 flower-like nanorods composite possesses the response value of 85 to 100 ppm ethanol vapor at 340 °C, indicating a great potential application of the synthesized sample to ethanol detection.

Table 1. The ethanol sensing performance of the previous reported results and this work.

Materials	Ethanol Vapor Concentration (ppm)	Temperature (°C)	Response (R_a/R_g)	Ref.
RGO/hollow SnO_2	100	300	70.4	[11]
Hollow ZnO/SnO_2 spheres	100	225	78.2	[16]
α-Fe_2O_3/g-C_3N_4	100	340	7.76	[29]
Au/3D SnO_2 microstructure	150	340	30	[38]
SnO_2/g-C_3N_4	100	340	85	this work

2.3. Mechanism Discussion

SnO_2 flower-like nanorods have been synthesized via a hydrothermal reaction method, and the schematic diagram of the synthesis of the g-C_3N_4 nanosheets-decorated SnO_2 flower-like nanorods is displayed in Figure 9. Many researchers hold the point that the diameter of the SnO_2 nanorods is changed by varying the Sn^+/OH^- ratio in solution [39]. However, Vuong et al. declared that the diameter of SnO_2 nanorods decreased with the increase of the stannic chloride amount. A proposed

growth mechanism of SnO_2 flower-like nanorods can be summarized by crystal growth and nucleation theory. The synthesis process includes two sections of nucleation and crystal growth. In the hydrothermal condition, the $Sn(OH)_6^{2-}$ nucleus is formed via the following chemical reactions in the process of nucleation stage [40]:

$$Sn^{4+} + 4OH^- \leftrightarrow Sn(OH)_4 \quad (1)$$

$$Sn(OH)_4 + 2OH^- \leftrightarrow Sn(OH)_6^{2-} \quad (2)$$

$$Sn(OH)_6^{2-} \rightarrow SnO_2 + H_2O + 2OH^- \quad (3)$$

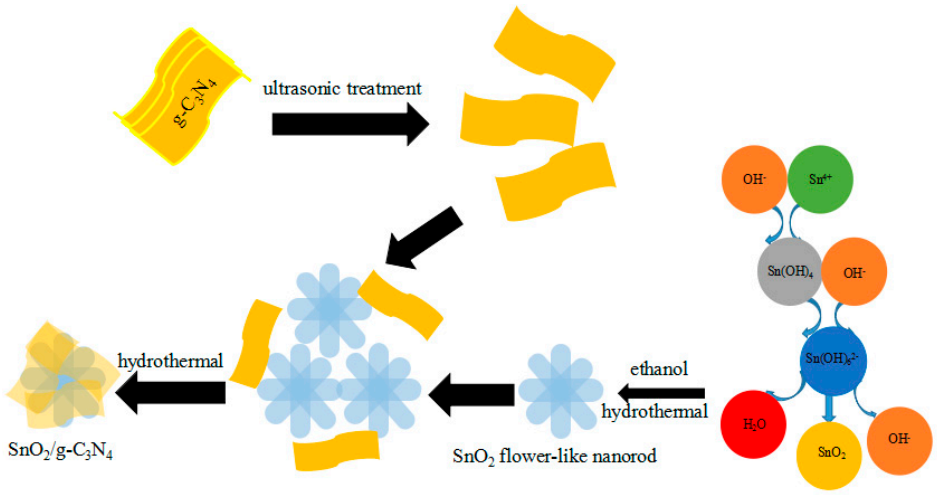

Figure 9. The schematic diagram of the synthesis of the g-C_3N_4 nanosheets decorated SnO_2 flower-like nanorods.

In the process, nucleation plays an important role not merely in the morphology formation but also in the quantity of the final product. At the initial stage of the chemical reaction, the Sn^{4+} ions start to react with the redundant OH^- ions and further form the $[Sn(OH)_6]^{2-}$ coordination ions. Meanwhile, a small quantity of SnO_2nanocrystals can be generated due to the decomposition of the $[Sn(OH)_6]^{2-}$ coordination ions. These initial SnO_2nanocrystals play an important role as seeds in the next hydrothermal stage. The $[Sn(OH)_6]^{2-}$ coordination ions could be accelerated to decompose and form plenty of SnO_2nanocrystals in the later hydrothermal reaction condition, which can be aggregated into SnO_2 nanoparticles. At the same time, these SnO_2 nanocrystals nucleation points around $[Sn(OH)_6]^{2-}$ can be oriented to grow into the rod-like structures. The SnO_2 nanocrystals nucleation points are generated in different orientations. As a result, the SnO_2 nanorods grow in irregular directions and finally form into 3D flower-like structures. This phenomenon can be explained by the fact that the surface-free energy of the rutile structure of crystalline SnO_2 faced an increase in the order of (110) < (100) < (101) < (001), which lead to the crystal growth on the faces of (001) or (101). However, the other faces have no exceptions [41,42].

2D g-C_3N_4 nanosheets-decorated SnO_2 flower-like nanorods composites were synthesized via a facile hydrothermal method as a high-property gas sensor for detecting ethanol. In order to understand the gas-sensing process, the schematic diagram of the test gas that reacted with SnO_2/g-C_3N_4 composite was shown in Figure 10a. As is known, the similar principle of gas sensor is the surface-adsorbed oxygen theory. When the sensor was exposed in the air condition, the oxygen molecules were adsorbed on the SnO_2 surface and capture electrons from the conduction band of SnO_2. Furthermore, the adsorbed oxygen molecules were ionized into O^{2-}, O^-, and O_2^- (Equation (4)), and formed a depletion layer with a certain width (W_s) of the hole accumulation (h^+) on the SnO_2 surface [43,44]. When the sensor was exposed in ethanol gas, the reduced gas ethanol

molecules were oxidized into acetaldehyde and finally turned into carbon dioxide and water by these oxygen anions (Equations (5) and (6)) [10]. As a result, the trapped electrons were released back to the SnO_2, depletion layer, where the width (W_s) of depletion area of the hole accumulation (h^+) became thinner and led to the decrease of the resistance by the transfer of electrons between ethanol molecules and oxygen anions. As is well known, the electrons transfer may affect the great change of the composite resistance. In addition, the improved ethanol-sensing performances of the g-C_3N_4 nanosheets-decorated flower-like SnO_2 nanorods composite could be attributed to the structure of SnO_2 nanorods coupled by 2D g-C_3N_4nanosheets and the heterojunction of interface region between flower-like SnO_2 nanorods and 2D g-C_3N_4.

$$O_2 + e^- \rightarrow O_2^- \quad (4)$$

$$2CH_3CH_2OH + O_2^- \rightarrow 2CH_3CHO + 2H_2O + e^- \quad (5)$$

$$2CH_3CHO + 5O_2^- \rightarrow 4CO_2 + 4H_2O + 5e^- \quad (6)$$

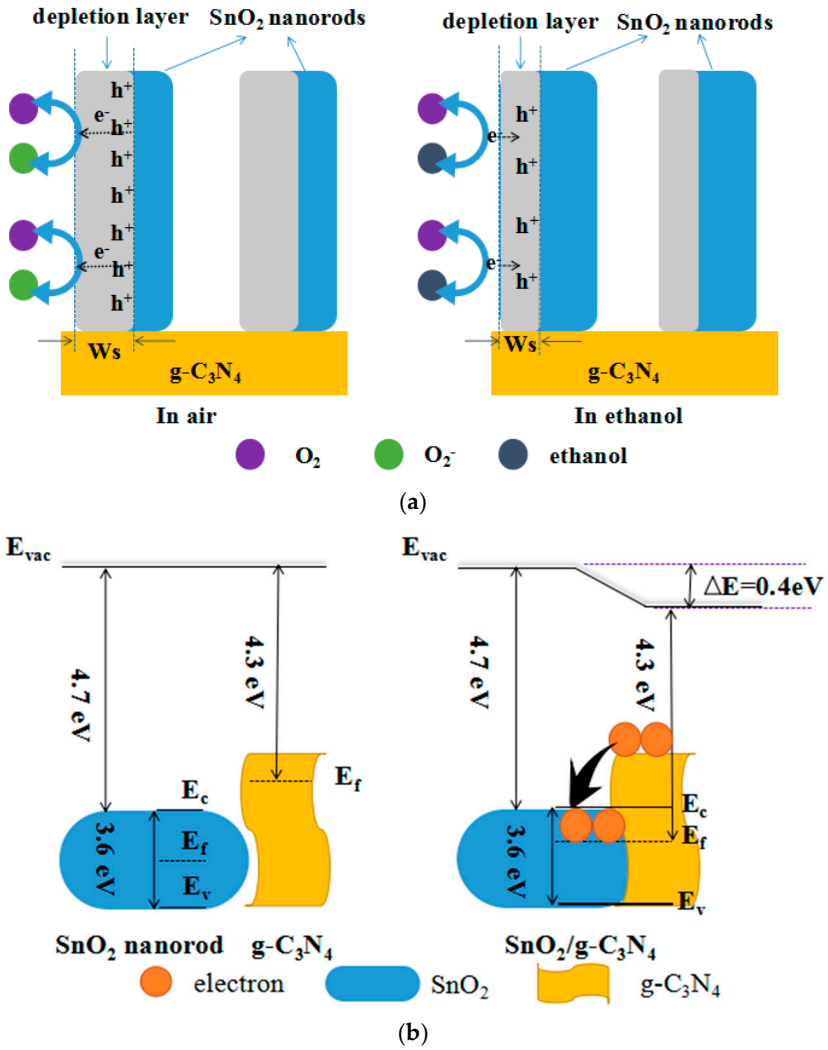

Figure 10. (**a**) The schematic diagram of air and ethanol react with the synthesized composite; and (**b**) the band diagram of SnO_2/g-C_3N_4 before and after the combination.

In general, the large specific area of 2D g-C_3N_4 nanosheets can provide more active sites to adsorb oxygen molecules and ethanol molecules. The interconnecting network structure created by

SnO_2 nanorods and 2D g-C_3N_4 nanosheets could supply more channels for the gas adsorption and diffusion and further enhance the interaction between SnO_2 and ethanol molecules. The energy band model (Figure 10b) was used to explain the energy change of SnO_2/g-C_3N_4 for ethanol detection. Figure 10b shows that the g-C_3N_4 and SnO_2 have the structure of valence band and conduction band (E_v and E_c) and the Fermi level (E_f) is between these two bands. When flower-like SnO_2 nanorods and 2D g-C_3N_4 nanosheetswere combined together, a heterojunction structure was formed. When ethanol molecules pass through the interface between g-C_3N_4 and SnO_2, the electrical property at the heterojunction was changed. SnO_2 and g-C_3N_4 are all n-type semiconductors with band gaps of 3.6 eV and 2.7 eV, respectively. Since the work function of g-C_3N_4 is smaller than that of SnO_2, the electrons will inflow from the conduction band of g-C_3N_4 to the conduction band of SnO_2, leading to a higher potential barrier. The fermi level is aligned when the electronic transmission achieves a new dynamic balance. The electrons may go over the low energy barriers and the schottky barrier is 0.4 eV. As a result, the electrons and holes are separated [27,43]. Meanwhile, the heterojunction structure may suppress the recombination of electron-hole and urge electrons to transfer quickly from ethanol vapour to the surface of SnO_2/g-C_3N_4. Therefore, this leads to a higher response because of the increased conductivity of the heterojunction structure [29].

3. Materials and Methods

3.1. Chemicals

Analytical-grade purity $SnCl_4 \cdot 5H_2O$ (99.0%), NaOH, and absolute ethyl alcohol were purchased from Shanghai Macklin Biochemical Co., Ltd, Shanghai, China and were used without further purification.

3.2. Sample Preparation

Graphitic carbon nitride (g-C_3N_4) was synthesized by our previous reported method [45]. Typically, 7 wt. % g-C_3N_4 nanosheets-decorated SnO_2 flower-like nanorods (SnO_2/g-C_3N_4-7) were synthesized by the hydrothermal method: 0.17 g g-C_3N_4 powder was dispersed into 200 mL ethanol under ultrasonic treatment for 2 h. 5.259 g $SnCl_4 \cdot 5H_2O$ was added into 200 mL of NaOH solution (0.81 M). Subsequently, the g-C_3N_4 solution was added into this mixture solution with magnetic stirring until it formed a white suspension. Finally, the mixture was transferred into a 500 mL stainless-steel Teflon-lined autoclave, then put into an oven and further heated at 200 °C for 48 h. The final product was washed with deionized water and ethanol several times and dried at 60 °C. According to this method, the SnO_2/g-C_3N_4 composites with 5 and 9 wt. % g-C_3N_4 content were also synthesized and marked as SnO_2/g-C_3N_4-5 and SnO_2/g-C_3N_4-9, respectively. The pure flower-like SnO_2nanorods were also synthesized by the same method.

3.3. Characterizations

X-ray diffraction (XRD) analysis was carried out on Bruker-AXS D8 (Bruker, Madison, WI, USA) with CuKα radiation at 40 kV and 25 mA. Fourier Transform Infrared Spectrometer (FT-IR) was recorded on a Bruker Tensor 27 (Bruker, Madison, WI, USA). Thermogravimetry (TG) analysis was completed on a NETZSCH STA449C Simultaneous Thermal Analyzer (NETZSCH, Selb, Germany) at a heating rate of 10 °C·min^{-1} under air atmosphere. Field-emission scanning electron microscopy (FESEM) (Quanta™ 250 FEG, FEI, Eindhoven, The Netherlands) was used to observe the structure and morphology of the sample. Transmission electron microscopy (TEM) analysis was done on a JEOL JEM-2100 microscope (JEOL, Tokyo, Japan) operating at 200 kV.

3.4. Gas Sensor Fabrication and Analysis

Gas-sensing performance test of the synthesized sample was carried out on an intelligent gas-sensing analysis system of CGS-4TPS (Beijing Elite Tech. Co., Ltd., Beijing, China). Figure 11 shows

the schematic diagram of the system, the sensor structure, and the working principle. In the sensor fabricate process, the synthesized sample was mixed with several drops of distilled water to form a paste. Then, a ceramic substrate (13.4 mm × 7 mm, screen-printed with Ag-Pd comb-like electrodes) was coated onto the paste to obtain the resistance-type sensor. Before the gas sensing test, the sensor was aged at 200 °C for 12 h to improve its stability and repeatability. In the sensing performance test process, the test gas was first injected into the closed 0.018 m^3 volume chamber by a microinjector with the relative humidity of 40%. The operating temperature was set in the range of 200 °C to 400 °C. The gas response (S) was defined as the ratio of *Ra*/*Rg*, where *Ra* and *Rg* were the resistances of sensor in air and in the test gas, respectively. The response and recovery times were defined as the time required for a change in response to reach 90% of the equilibrium value.

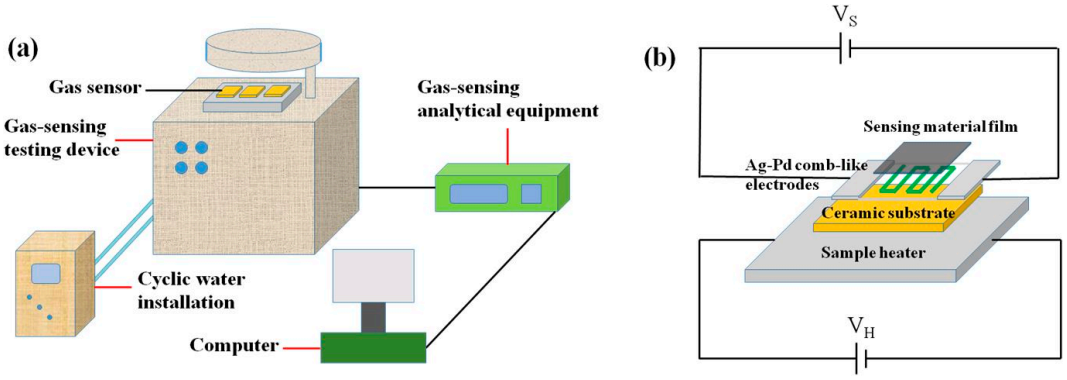

Figure 11. (**a**) The schematic diagram of the CGS-4TPS gas-sensing test system and (**b**) the gas sensor structure.

4. Conclusions

In summary, the g-C_3N_4 nanosheets-decorated tin oxide flower-like nanorods (SnO_2/g-C_3N_4) composite was successfully synthesized by using a facile hydrothermal method. The as-prepared sample possesses flower-like nanorods and a lamellar structure. Compared with pure SnO_2, the g-C_3N_4 nanosheets-decorated SnO_2 flower-like nanorods exhibited an obvious improvement of gas sensing performance to ethanol, and the response value was 150 to 500 ppm ethanol at 340 °C. The improved sensing properties are mainly attributed to the high surface area of the sample and the heterojunction between SnO_2 and g-C_3N_4. Considering the effective synthesis approach and the high sensing performance, the as-prepared SnO_2/g-C_3N_4 composite could be an ideal candidate for ethanol detection application.

Acknowledgments: This work was supported by the National Natural Science Foundation of China (51404097, 51504083, U1404613), Natural Science Foundation of Henan Province of China (162300410113), Program for Science & Technology Innovation Talents in Universities of Henan Province (17HASTIT029, 18HASTIT010), Project funded by China Postdoctoral Science Foundation (2016M592290), the Research Foundation for Youth Scholars of Higher Education of Henan Province (2016GGJS-040), the Fundamental Research Funds for the Universities of Henan Province (NSFRF1606,NSFRF1614), Program for Innovative Research Team in University of Ministry of Education of China (IRT_16R22), Foundation for Distinguished Young Scientists of Henan Polytechnic University (J2016-2, J2017-3), and the State Key Laboratory Cultivation Base for Gas Geology and Gas Control (Henan Polytechnic University) (WS2017A03).

Author Contributions: Yan Wang conceived and designed the experiments; Bo Zhang, Guang Sun, and Zhanying Zhang performed the experiments and analyzed the data; Jianliang Cao and Cong Qin provided the concept of this research and managed all the experimental and writing process as the corresponding authors; all authors discussed the results and commented on the manuscript.

Conflicts of Interest: The authors declare no conflict of interest.

References

1. Shi, Y.H.; Ma, D.Q.; Wang, W.J.; Zhang, L.F.; Xu, X.H. A supramolecular self-assembly hydrogel binder enables enhanced cycling of SnO_2-based anode for high-performance lithium-ion batteries. *J. Mater. Sci.* **2017**, *52*, 3545–3555. [CrossRef]
2. Akhundi, A.; Habibiyangjeh, A. A simple large-scale method for preparation of g-C_3N_4/SnO_2 nanocomposite as visible-light-driven photocatalyst for degradation of an organic pollutant. *Mater. Express* **2015**, *5*, 309–318. [CrossRef]
3. Zhang, J.; Liu, X.H.; Neri, G.; Pinna, N. Nanostructured Materials for Room-Temperature Gas Sensors. *Adv. Mater.* **2016**, *28*, 795–831. [CrossRef] [PubMed]
4. Das, S.; Jayaraman, V. SnO_2: A Comprehensive Review on Structures and Gas Sensors. *Prog. Mater. Sci.* **2014**, *66*, 112–255. [CrossRef]
5. Wu, M.Y.; Zeng, W.; Li, Y.Q. Hydrothermal synthesis of novel SnO_2 nanoflowers and their gas-sensing properties. *Mater. Lett.* **2013**, *104*, 34–36. [CrossRef]
6. Luo, L.; Jiang, Q.P.; Qin, G.H.; Zhao, K.; Du, G.F.; Wang, H.; Zhao, H.Y. Gas sensing characteristics of novel twin-layered SnO_2 nanoarray fabricated by substrate-free hydrothermal route. *Sens. Actuators B* **2015**, *218*, 205–214. [CrossRef]
7. Zhang, J.; Wu, J.J.; Wang, X.X.; Zeng, D.W.; Xie, C.S. Enhancing room-temperature NO_2 sensing properties via forming heterojunction for NiO-rGO composited with SnO_2 nanoplates. *Sens. Actuators B* **2016**, *243*, 1010–1019. [CrossRef]
8. Choi, S.W.; Katoch, A.; Kim, J.H.; Kim, S.S. Striking sensing improvement of n-type oxide nanowires by electronic sensitization based on work function difference. *J. Mater. Chem. C* **2015**, *3*, 1521–1527. [CrossRef]
9. Zhang, H.; Zeng, W.; Hao, J.H.; Li, Y.Q.; Miao, B. Hydrothermal synthesis of flower-like SnO_2 architectures with superior gas sensing properties. *Mater. Lett.* **2015**, *145*, 133–136. [CrossRef]
10. Zhang, D.Z.; Liu, J.J.; Chang, H.Y.; Liu, A.M.; Xia, B.K. Characterization of a hybrid composite of SnO_2 nanocrystal-decorated reduced graphene oxide for ppm-level ethanol gas sensing application. *RSC Adv.* **2015**, *5*, 18666–18672. [CrossRef]
11. Zito, C.A.; Perfecto, T.M.; Volanti, D.P. Impact of reduced graphene oxide on the ethanol sensing performance of hollow SnO_2 nanoparticles under humid atmosphere. *Sens. Actuators B* **2017**, *244*, 466–474. [CrossRef]
12. Feng, Q.X.; Li, X.G.; Wang, J. Percolation effect of reduced graphene oxide (rGO) on ammonia sensing of rGO-SnO_2 composite based sensor. *Sens. Actuators B* **2017**, *243*, 1115–1126. [CrossRef]
13. Song, Z.L.; Wei, Z.R.; Wang, B.C.; Luo, Z.; Xu, S.M.; Zhang, W.K.; Yu, H.X.; Li, M.; Huang, Z.; Zang, J.F.; et al. Sensitive room-temperature H_2S gas sensors employing SnO_2 quantum wire/reduced graphene oxide nanocomposites. *Chem. Mater.* **2016**, *28*, 1205–1212. [CrossRef]
14. Mao, S.; Cui, S.M.; Lu, G.H.; Yu, K.H.; Wen, Z.H.; Chen, J.H. Tuning gas-sensing properties of reduced graphene oxide using tin oxide nanocrystals. *J. Mater. Chem.* **2012**, *22*, 11009–11013. [CrossRef]
15. Zhang, H.; Feng, J.C.; Fei, T.; Liu, S.; Zhang, T. SnO_2 nanoparticles-reduced graphene oxide nanocomposites for NO_2 sensing at low operating temperature. *Sens. Actuators B* **2014**, *190*, 472–478. [CrossRef]
16. Liu, J.Y.; Wang, T.S.; Wang, B.Q.; Sun, P.; Yang, Q.Y.; Liang, X.S.; Song, H.W.; Lu, G.Y. Highly sensitive and low detection limit of ethanol gas sensor based on hollow ZnO/SnO_2 spheres composite material. *Sens. Actuators B* **2017**, *245*, 551–559. [CrossRef]
17. Poloju, M.; Jayababu, N.; Manikandan, E.; Ramana Reddy, M.V. Enhancing the Isopropanol gas sensing performance of SnO_2/ZnO core/shell nanocomposite gas sensor. *J. Mater. Chem. C* **2017**, *5*, 2662–2668. [CrossRef]
18. Silva, L.F.D.; M'Peko, J.-C.; Catto, A.C.; Bernardini, S.; Mastelaro, V.R.; Aguir, K.; Ribriro, C.; Longo, E. UV-enhanced ozone gas sensing response of ZnO-SnO_2 heterojunctions at room temperature. *Sens. Actuators B* **2017**, *240*, 573–579. [CrossRef]
19. Wang, L.W.; Li, J.T.; Wang, Y.H.; Yu, K.F.; Tang, X.Y.; Zhang, Y.Y.; Wang, S.P.; Wei, C.S. Construction of 1D SnO_2-coated ZnO nanowire heterojunction for their improved n-butylamine sensing performances. *Sci. Rep.* **2016**, *6*, 35079. [CrossRef] [PubMed]
20. Choi, K.S.; Park, S.; Chang, S.P. Enhanced ethanol sensing properties based on SnO_2 nanowires coated with Fe_2O_3 nanoparticles. *Sens. Actuators B* **2017**, *238*, 871–879. [CrossRef]

21. Wang, T.S.; Huang, Z.S.; Yu, Z.D.; Wang, B.Q.; Wang, H.; Sun, P.; Suo, H.; Gao, Y.; Sun, Y.F.; Li, T.; et al. Low operating temperature toluene sensor based on novel α-Fe_2O_3/SnO_2 heterostructure nanowire arrays. *RSC Adv.* **2016**, *6*, 52604–52610. [CrossRef]
22. Sun, P.; Wang, C.; Liu, J.G.; Zhou, X.; Li, X.W.; Hu, X.L.; Lu, G.Y. Hierarchical assembly of α-Fe_2O_3 nanosheets on SnO_2 hollow nanospheres with enhanced ethanol sensing properties. *ACS Appl. Mater. Interface* **2015**, *7*, 19119–19125. [CrossRef] [PubMed]
23. Yu, Q.X.; Zhu, J.H.; Xu, Z.Y.; Huang, X.T. Facile synthesis of α-Fe_2O_3@SnO_2 core–shell heterostructure nanotubes for high performance gas sensors. *Sens. Actuators B* **2015**, *213*, 27–34. [CrossRef]
24. Gu, C.P.; Cui, Y.W.; Wang, L.Y.; Sheng, E.H.; Shim, J.J.; Huang, J.R. Synthesis of the porous NiO/SnO_2 microspheres and microcubes and their enhanced formaldehyde gas sensing performance. *Sens. Actuators B* **2017**, *241*, 298–307. [CrossRef]
25. Wang, Y.; Zhang, H.; Sun, X.H. Electrospun Nanowebs of NiO/SnO_2 p-n Heterojunctions for Enhanced Gas Sensing. *Appl. Surf. Sci.* **2016**, *389*, 514–520. [CrossRef]
26. Zhang, J.; Zeng, D.W.; Zhu, Q.; Wu, J.J.; Huang, Q.W.; Zhang, W.; Xie, C.S. Enhanced room temperature NO_2 response of NiO-SnO_2 nanocomposites induced by interface bonds at the p-n heterojunction. *Phys. Chem. Chem. Phys.* **2016**, *18*, 5386–5396. [CrossRef] [PubMed]
27. Zang, Y.P.; Li, L.P.; Li, X.G.; Lin, R.; Li, G.S. Synergistic collaboration of g-C_3N_4/SnO_2 composites for enhanced visible-light photocatalytic activity. *Chem. Eng. J.* **2014**, *246*, 277–286. [CrossRef]
28. Chen, X.; Zhou, B.H.; Yang, S.L.; Wu, H.S.; Wu, Y.X.; Wu, L.D.; Pan, J.; Xiong, X. In situ construction of an SnO_2/g-C_3N_4 heterojunction for enhanced visible-light photocatalytic activity. *RSC Adv.* **2015**, *5*, 68953–68963. [CrossRef]
29. Zhang, Y.J.; Zhang, D.K.; Guo, W.M.; Chen, S.J. The α-Fe_2O_3/g-C_3N_4 heterostructural nanocomposites with enhanced ethanol gas sensing performance. *J. Alloys Compd.* **2016**, *685*, 84–90. [CrossRef]
30. Zeng, B.R.; Zhang, L.C.; Wan, X.Y.; Song, H.J.; Lv, Y. Fabrication of α-Fe_2O_3/g-C_3N_4 composites for cataluminescence sensing of H_2S. *Sens. Actuators B* **2015**, *211*, 370–376. [CrossRef]
31. Hu, Y.; Li, L.; Zhang, L.C.; Lv, Y. Dielectric barrier discharge plasma-assisted fabrication of g-C_3N_4-Mn_3O_4 composite for high-performance cataluminescence H_2S gas sensor. *Sens. Actuators B* **2017**, *239*, 1177–1184. [CrossRef]
32. Mathur, S.; Barth, S.; Shen, H.; Pyun, J.-C.; Werner, U. Size-Dependent Photoconductance in SnO_2 Nanowires. *Small* **2005**, *1*, 713–717. [CrossRef] [PubMed]
33. Kuang, Q.; Lao, C.S.; Wang, Z.L.; Xie, Z.X.; Zheng, L.S. High-sensitivity humidity sensor based on a single SnO_2 nanowire. *J. Am. Chem. Soc.* **2007**, *129*, 6070–6071. [CrossRef] [PubMed]
34. Paulowicz, I.; Hrkac, V.; Kaps, S.; Cretu, V.; Lupan, O.; Braniste, T.; Duppel, V.; Tiginyanu, L.; Kienle, L.; Adelung, R.; et al. Nanowire Networks: Three-Dimensional SnO_2 Nanowire Networks for Multifunctional Applications: From High-Temperature Stretchable Ceramics to Ultraresponsive Sensors. *Adv. Electron. Mater.* **2015**, *1*, 1500081. [CrossRef]
35. Lupan, O.; Braniste, T.; Deng, M.; Ghimpu, L.; Paulowicz, I.; Mishra, Y.K.; Kienle, L.; Adelung, R.; Tiginyanu, I. Rapid switching and ultra-responsive nanosensors based on individual shell–core Ga_2O_3/GaN:O_x@SnO_2 nanobelt with nanocrystalline shell in mixed phases. *Sens. Actuators B* **2015**, *221*, 544–555. [CrossRef]
36. Dai, H.; Zhang, S.P.; Xu, G.F.; Peng, Y.R.; Gong, L.S.; Li, X.H.; Li, Y.L.; Lin, Y.Y.; Chen, G.N. Highly photoactive heterojunction based on g-C_3N_4 nanosheets decorated with dendritic zinc(II) phthalocyanine through axial coordination and its ultrasensitive enzyme-free sensing of choline. *RSC Adv.* **2014**, *4*, 58226–58230. [CrossRef]
37. Xiao, Y.; Yang, Q.Y.; Wang, Z.Y.; Zhang, R.; Gao, Y.; Sun, P.; Sun, Y.F.; Lu, G.Y. Improvement of NO_2 gas sensing performance based on discoid tin oxide modified by reduced graphene oxide. *Sens. Actuators B* **2016**, *227*, 419–426. [CrossRef]
38. Guo, J.; Zhang, J.; Gong, H.B.; Ju, D.X.; Cao, B.Q. Au nanoparticle-functionalized 3D SnO_2 microstructures for high performance gas sensor. *Sens. Actuators B* **2016**, *226*, 266–272. [CrossRef]
39. Lupan, O.; Chow, L.; Chai, G.; Heinrich, H.; Park, S.; Schulte, A. Synthesis of one-dimensional SnO_2 nanorods via a hydrothermal technique. *Physica E* **2009**, *41*, 533–536. [CrossRef]
40. Vuong, D.D.; Hien, V.X.; Trung, K.Q.; Chien, N.D. Synthesis of SnO_2 micro-spheres, nano-rods and nano-flowers via simple hydrothermal route. *Physica E* **2011**, *44*, 345–349. [CrossRef]
41. Cheng, B.; Russell, J.M.; Shi, W.S.; Zhang, L.; Samulski, E.T. Large-Scale, Solution-Phase Growth of Single-Crystalline SnO_2 Nanorods. *J. Am. Chem. Soc.* **2004**, *126*, 5972–5973. [CrossRef] [PubMed]

42. Liu, Y.L.; Huang, J.; Yang, J.D.; Wang, S.R. Pt nanoparticles functionalized 3D SnO_2 nanoflowers for gas sensor application. *Solid State Electron.* **2017**, *130*, 20–27. [CrossRef]
43. Chen, Y.; Zhang, W.; Wu, Q.S. A highly sensitive room-temperature sensing material for NH_3: SnO_2-nanorods coupled by rGO. *Sens. Actuators B* **2017**, *242*, 1216–1226. [CrossRef]
44. Zhang, Z.Y.; Zhu, L.P.; Wen, Z.; Ye, Z.Z. Controllable synthesis of Co_3O_4 crossed nanosheet arrays toward an acetone gas sensor. *Sens. Actuators B* **2017**, *238*, 1052–1059. [CrossRef]
45. Cao, J.L.; Qin, C.; Wang, Y.; Zhang, B.; Gong, Y.X.; Zhang, H.L.; Sun, G.; Hari, B.; Zhang, Z.Y. Calcination Method Synthesis of SnO_2/g-C_3N_4 Composites for a High-Performance Ethanol Gas Sensing Application. *Nanomaterials* **2017**, *7*, 98. [CrossRef] [PubMed]